Journal of Groundwater Science and Engineering
ISSN 2305-7068
Indexed by ESCI CABI CSA
Scopus GeoRef AJ CNKI

Experimental and numerical investigation of groundwater head losses on and nearby short intersections between disc-shaped fractures

Ci-xiao Qu, Ming-yu Wang, Peng Wang

Citation:
Qu CX, Wang MY, Wang P. 2022. Experimental and numerical investigation of groundwater head losses on and nearby short intersections between disc-shaped fractures. Journal of Groundwater Science and Engineering, 10(1): 33-43.

View online: https://doi.org/10.19637/j.cnki.2305-7068.2022.01.004

Articles you may be interested in

Experimental and numerical investigation for energy dissipation of supercritical flow in sudden contractions
Journal of Groundwater Science and Engineering. 2020, 8(4): 396-406 https://doi.org/10.19637/j.cnki.2305-7068.2020.04.009

Research on numerical simulation of the groundwater funnels restoration in Shijiazhuang
Journal of Groundwater Science and Engineering. 2018, 6(2): 126-135

Numerical simulation of response of groundwater flow system in inland basin to density changes
Journal of Groundwater Science and Engineering. 2018, 6(1): 7-17 https://doi.org/10.19637/j.cnki.2305-7068.2018.01.002

Numerical analysis and evaluation of groundwater recession in a flood detention basin
Journal of Groundwater Science and Engineering. 2019, 7(3): 253-263 https://doi.org/DOI: 10.19637/j.cnki.2305-7068.2019.03.006

Study on numerical simulation of organic pollutant transport in groundwater northwest of Laixi
Journal of Groundwater Science and Engineering. 2018, 6(4): 293-305 https://doi.org/10.19637/j.cnki.2305-7068.2018.04.005

Numerical investigation of hydraulic characteristics and prediction of cavitation number in Shahid Madani Dam's Spillway
Journal of Groundwater Science and Engineering. 2019, 7(4): 323-332 https://doi.org/DOI: 10.19637/j.cnki.2305-7068.2019.04.003

Journal homepage: http://gwse.iheg.org.cn

Experimental and numerical investigation of groundwater head losses on and nearby short intersections between disc-shaped fractures

Ci-xiao Qu[1], Ming-yu Wang[1*], Peng Wang[1]

[1] *College of Resources and Environment*, *University of Chinese Academy of Sciences*, *Beijing* 100049, *China*.

Abstract: Discrete fracture models are used for investigating precise processes of groundwater flow in fractured rocks, while a disc-shaped parallel-plates model for a single fracture is more reasonable and efficient for computational treatments. The flow velocity has a large spatial differentiation which is more likely to produce non-linear flow and additional head losses on and nearby intersections in such shaped fractures, therefore it is necessary to understand and quantify them. In this study, both laboratory experiments and numerical simulations were performed to investigate the total head loss on and nearby the intersections as well as the local head loss exactly on the intersections, which were not usually paid sufficient attention or even ignored. The investigation results show that these two losses account for 29.17%-84.97% and 0-73.57% of the entire total head loss in a fracture, respectively. As a result, they should be necessarily considered for groundwater modeling in fractured rocks. Furthermore, both head losses become larger when aperture and flow rate increase and intersection length decreases. Particularly, the ratios of these two head losses to the entire total head loss in a fracture could be well statistically explained by power regression equations with variables of aperture, intersection length, and flow rates, both of which achieved high coefficients of determination. It could be feasible through this type of study to provide a way on how to adjust the groundwater head from those obtained by numerical simulations based on the traditional linear flow model. Finally, it is practicable and effective to implement the investigation approach combining laboratory experiments with numerical simulations for quantifying the head losses on and nearby the intersections between disc-shaped fractures.

Keywords: Groundwater head losses; Disc-shaped Fracture; Laboratory experiments; Numerical simulations; Short intersections

Received: 12 Jul 2021/ Accepted: 28 Dec 2021

2305-7068/© 2022 Journal of Groundwater Science and Engineering Editorial Office

Introduction

Fractures usually serve as preferential conduits (Pruess, 1998; Su et al. 2001; Borgne et al. 2006; Reza et al. 2018) for fluid flow and solute transport compared with the matrix of relatively low permeability. Generally, discrete fracture models (Dverstorp et al. 1992; Cacas, 1990; Wang et al. 2002; Hartley and Roberts, 2013; Lei et al. 2017; Wang et al. 2020) are used to investigate the mechanisms and characteristics of groundwater flow and transport, especially in laboratory experiments and numerical simulations. The flow velocity in a fracture is relatively high and it presents with a large spatial differentiation on the fracture plane, which is more likely to produce non-linear flow and additional head losses on both contacts and intersections in fractures that are usually ignored. The previous studies usually conceptualized a fracture as rectangular parallel plates or a 1-D pipe (Wilson and Witherspoon, 1976; Witherspoon et al. 1980; Kolditz, 2001; Zimmerman et al. 2004; Hu YJ et al. 2005; Johnson J et al. 2006; Zhang et al. 2013), which did not focus on the difference of the velocity distribution on the entire fracture plane. However, such velocity distribution, which may be related with the fracture shape and the intersection length, results in dominant flow area and local strong turbulence area where there are often addi-

*Corresponding author: Ming-yu Wang, *E-mail address*: mwang@ucas.edu.cn

DOI: 10.19637/j.cnki.2305-7068.2022.01.004

Qu CX, Wang MY, Wang P. 2022. Experimental and numerical investigation of groundwater head losses on and nearby short intersections between disc-shaped fractures. Journal of Groundwater Science and Engineering, 10(1): 33-43.

tional head losses.

For either laboratory experiments or numerical simulations, it is firstly needed to conceptualize the fracture as a reasonable geometric shape. For a tensile natural fracture in an isotropic and homogeneous rock, its shape or at least its initial shape, tends to be irregular circle or ellipse (Jing, 2007). The circle shape might be quickly deformed into irregular shapes (like polygons) by successive tectonic movements. As a result, a few scholars applied the polygon models in their researches (Dershowitz et al. 1988; Koudina et al. 1998; Tuckwell et al. 2003). However, the irregular shapes are difficult for computational idealization. Therefore, many researchers (Pollard, 1976; Baecher and Lanney, 1978; Long et al. 1985; Wang et al. 2002; Vu et al. 2018; Guo et al. 2020) preferred to adopt the round or elliptic fracture models not only because these models are tractable but also some investigations showed that some flow or rock mechanical properties originally developed from disc-shaped fractures remain valid for arbitrary fracture shapes (Grechka, 2006). It is commonly agreed that a fracture would be cut by many other adjacent fractures in a fracture network, either circle, ellipse or polygons could present similar geometrical features and fluid flow behaviors (such as velocity spatial differentiation). To facilitate the calculation of geometric parameters, the disc-shape was taken for investigating the different types of groundwater head losses through laboratory experiments and numerical analysis in this paper.

The estimation of non-linear head losses especially the local head losses on the fracture intersections needs to be further clarified. Indeed, the groundwater hydraulic data sometimes could be reproduced by certain professional numerical simulation packages which are based on linear laminar flow hypothesis when the flow rate is relatively low. Those modeling packages include, for examples, Hydrogeosphere (HGS), Groundwater Modeling System (GMS), and Transport of Unsaturated Groundwater and Heat (TOUGH). Some other numerical software for performing non-linear fluid-dynamic calculations such as Computational Fluid Dynamics (CFD) and Ansys Fluent (Petchsingto and Karpyn, 2009; Liu et al. 2016; Gong et al. 2020; Xiong et al. 2020) could not compute groundwater flow and solute transport in complex subsurface media (like dual media coupling) with sophisticated hydrogeological boundary conditions. Only very few numerical simulation packages such as COMSOL could be applied to perform the non-linear processes along the flow path (Cao et al. 2019), however, it is a heavy burden for personal computer even workstation to model a turbulent transient flow in a complex discrete fracture network.

In fact, if there are simplified statistical models which could reasonably describe the relationships of the additional head loss produced on some crucial positions in a fracture with its primary pertaining parameters, it will be more efficient and feasible for most researchers to carry out practical work. These statistical relationships could also be used to improve the existing linear flow simulations in a more precise and efficient way. Furthermore, it can also be applied to the dimensionality reduction algorithms (Wang et al. 2002) for simplified conceptualization of discrete fracture network. Wang et al. (2002) conceptualized a fracture plane to several connected 1-D pipes, and assigned the equivalent parameters to the segments or on the nodes to comprehensively represent the spatial differences of pertaining parameters on the plane. This method could be extended to non-linear regime by assigning equivalent additional head losses derived from the statistical models to nodes at pipe ends based on an appropriate algorithm.

In this study, both laboratory experiments and numerical simulations were performed to investigate additional head losses including the total head loss on and nearby the intersections between disc-shaped fractures as well as the local head loss exactly on the intersections, which were not usually paid sufficient attention or even ignored. It should be pointed out that the shorter intersection lengths were particularly considered in this study in which the discrepancy of the velocity distribution would be more obvious in a whole fracture disk to make the additional head losses more meaningful.

1 The laboratory experiment design and the numerical simulation model

1.1 Setup and design for the laboratory experiments

In this study, a disc-shaped setup made up of two smooth parallel plexiglass plates was applied to simulate a single disc-shaped fracture, and two symmetrical water tanks connected to the ‘fracture’ were used to control the inflow and outflow boundary conditions (Fig. 1). The intersecting cross-section between the ‘fracture’ and two water tanks are defined as the inlet and outlet, respectively. The length of intersections (L) can be adjusted by blocking with plugs of different sizes. The dia-

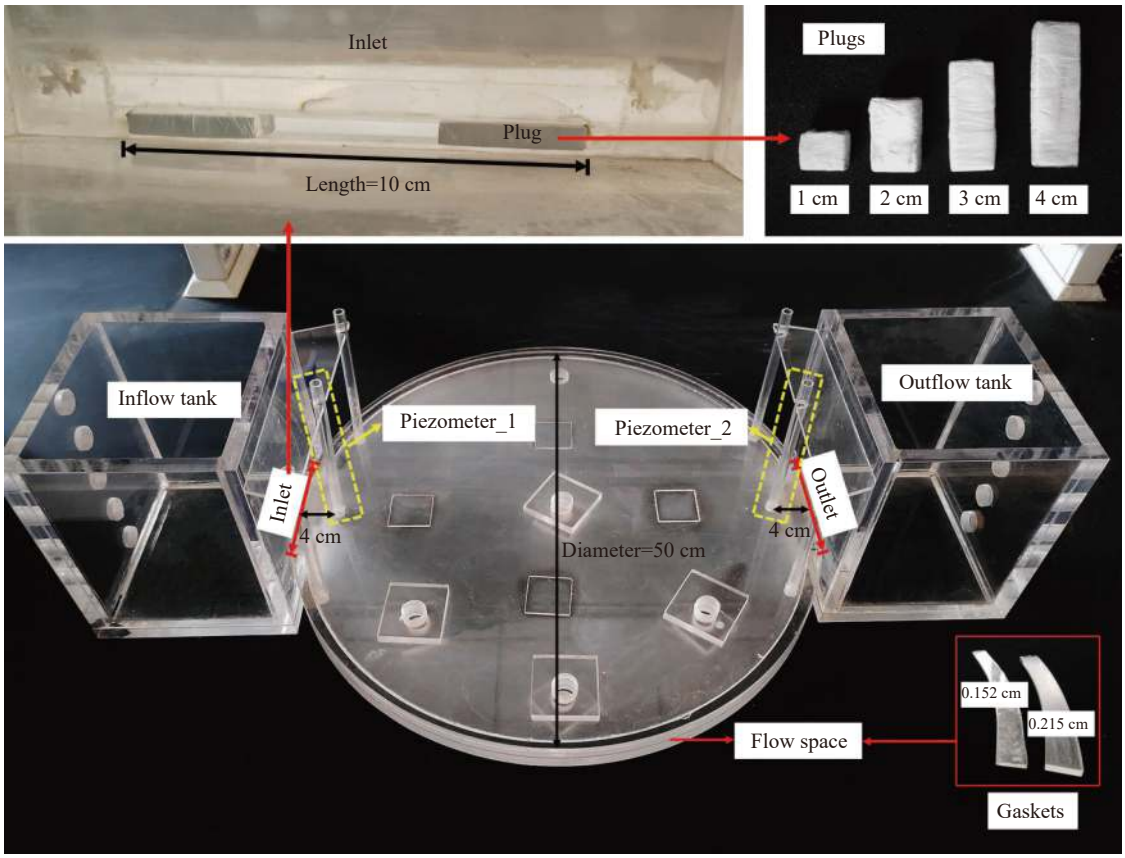

Fig. 1 The physical laboratory setup of disc-shaped fracture

meter of this disc-shaped fracture is 50 cm and there are two piezometer pipes on the midline, 4 cm away from the inlet and outlet, respectively. Besides, the distance between the two parallel plates (called as aperture b) could be changed flexibly by putting different gaskets into the gap between the two parallel planes to create different aperture scenarios.

Each hydrodynamic experiment was performed in a steady state with a constant flow rate (Q) implemented by a peristaltic pump (LeadFluid, Model JP300S, China). The observed heads in two tanks (H_{in_exp} and H_{out_exp}) were regarded as the total heads, because the velocity head in tank is of smaller orders of magnitude compared with the total head so it can be ignored. Moreover, the total head loss ($\Delta H_{p1-2\_exp} = H_{p1\_exp} - H_{p2\_exp}$) is approximately equal to the head loss between the two head values measured through the two piezometer pipes as the flow rates at these two positions are similar.

When 2 different apertures (b (cm) = 0.152, 0.215) and 4 different intersection lengths (L (cm) = 10, 8, 6, 4) were considered, the physical laboratory setup would be adjusted into 8 structure states. In each structure state, the flow experiments were conducted with 5 different flow rates while the water temperature remained from 22℃ to 23℃. Totally, 40 different scenarios were established in this study.

1.2 Numerical simulation package and model setup

The HydroGeoSphere (HGS) modeling package, developed by Edward Sudicky et al. from the University of Waterloo, was used to simulate the fluid flow within a fracture by using the discrete fracture module. In HGS, linear flow equation (Bear, 1972) was used in the fractured domain assuming the fractures are non-deformable and the fluid is incompressible. As a result, it is assumed that the linear flow condition presents without considering the turbulence and the local head loss. The controlling equations are given as follows:

$$q_f = -K_f \cdot k_{rf} \overline{\overline{\nabla}} (\psi_f + z_f) \tag{1}$$

$$K_f = \frac{\rho g b^2}{12\mu} \tag{2}$$

Where: q_f is fluid flow rate [LT^{-1}] in a fracture; $\overline{\overline{\nabla}}$ is the two-dimensional gradient operator defined on the fracture plane; K_f is the saturated hydraulic conductivity of a fracture [LT^{-1}]; k_{rf} is the relative

permeability of the fracture [dimensionless]; ψ_f and z_f are the pressure and the elevation heads, respectively, within the fracture [L]; ρ is the density of water [ML^{-3}]; g is the gravitational acceleration [LT^{-2}]; b is the aperture of fracture [L] and μ is the viscosity of water [$ML^{-1}T^{-1}$].

The numerical fracture flow models (Fig. 2), in which the corresponding parameter values taken from the experimental scenarios were assigned to b, μ, and so on (Table 1), were built with HGS. Additionally, the modelling domain was discretized with grid size of 0.2 cm in both x and y directions. In these numerical models, the matrix was set to be impermeable and the fluid only flowed within the fractured domain in a stead state. The inlet and outlet were defined as specified flux boundaries and a constant head boundary was placed at the cell where observation point of piezometer_1 was located.

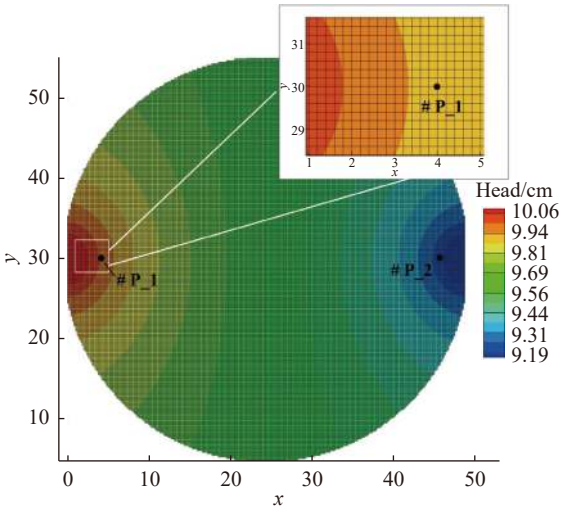

Fig. 2 The numerical representation of a disc-shaped fracture in HGS

2 Experimental and numerical simulation results along with analysis and discussion

In general, the head loss, which occurs along a flow path and is correlated to the path length, is defined as major head loss (frictional head loss), and the friction factors controlling the flow status from laminar to turbulent regime is usually obtained from the Moody Chart (Moody and Princeton 1944; Kemler, 1933; Hunter, 1946). Minor head loss (local head loss) occurs due to bends, elbows, joints, valves, etc.

$$H_f = f\frac{L}{D}\frac{v^2}{2g}(Major\ head\ loss) \quad (3)$$

$$H_f = k\frac{v^2}{2g}(Minor\ head\ loss) \quad (4)$$

Where: H_f is the frictional head loss [L]; f is the friction factor [dimensionless]; L is the length of pipe [L]; D is the diameter of pipe [L]; v is the fluid velocity [LT^{-1}]; g is the gravitational acceleration [LT^{-2}] and k is the loss coefficient [dimensionless].

It should be noted that those equations are derived from pipe flow. In order to further explore the head losses in fracture network, the new definitions of the head losses in fractures, which are different from the their traditional classification mentioned above are given as follows: (1) the head loss ΔH_l occurs in the linear laminar flow along the flow path, which could be obtained from numerical simulations; (2) the head loss ΔH_n occurs in non-linear flow along the flow path representing the non-linear part, and the sum of ΔH_l and ΔH_n is the traditional frictional head loss; (3) the local head loss ΔH_i occurs on the intersections of the fractures. Compared with the linear loss ΔH_l, ΔH_n and ΔH_i cause the non-linear losses together, so these two parts could be defined as additional head loss. The schematic diagram of these three losses is shown in Fig. 3.

2.1 Total head losses occurred on and nearby the intersections

Based on the experimental design, a number of flow experiments were conducted, from which

Table 1 The parameters assigned in the corresponding numerical models

Parameters	Units	Values
Boundary (flow in and flow out) Length (L)	cm	10, 8, 6, 4 corresponding with each experiment
Specified flux (Q)	cm^3/s	corresponding with each experiment
Aperture (b)	cm	0.215, 0.125 corresponding with each experiment
Reference fluid density (ρ)	kg/cm^3	9.98E-4
Reference fluid viscosity (μ)	kg/(cm·s)	9.53E-6
Acceleration due to gravity (g)	cm/s^2	9.81E+2

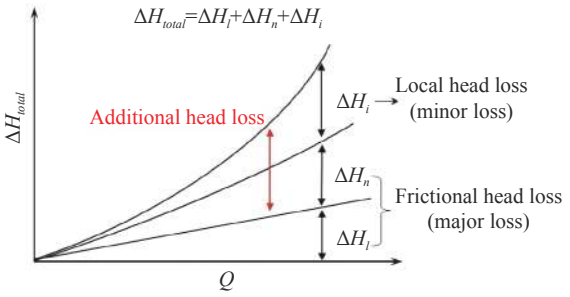

Fig. 3 The schematic diagram of three losses (H_l, H_n and H_i) defined in this paper

H_{in_exp}, H_{out_exp}, H_{p1_exp} and H_{p2_exp} were recorded. It should be noted that ΔH_{in-out_exp} represents the total head loss within the whole setup in each flow experiment. ΔH_{s_exp} is the difference between ΔH_{in-out_exp} and ΔH_{p1-2_exp}, representing the total head loss within the two regions , i.e. from the inlet to piezometer pipe_1 and from piezometer pipe_2 to the outlet, both are about one sixth of total flow path.

Fig. 4 shows the relationships between the hydraulic gradient (∇H_{in-out_exp} and ∇H_{p1-2_exp}) and the flow rates (Q) in different experimental scenarios. It can be seen that the nonlinear relationship between ∇H_{total} and Q becomes more obvious with the increase of b and the decrease of L, especially for $Q \sim \nabla H_{in-out\_exp}$, which indicates that additional losses would have occurred.

From Table 2 and Fig. 5, it is interesting to note that ΔH_{s_exp} may account for a very large proportion of ΔH_{in-out_exp} (29.17% - 84.97%) although it was produced within a rather short segment compared with the whole flow path covering a small seepage area.

With the increase of b and Q, and the decrease of L, this proportion consistently presents an increasing trend. After attempting several possible functions types (e.g. linear, exponential, logarithmic, polynomial, power function, etc.), it was found that the product of power function is the best fit. By conducting the nonlinear regression analysis of this proportion with those three impact variables, the power function in Equation (5) was obtained with a rather high coefficient of determination equal to 0.958. This indicates that the shrinkage of the flow path caused by the specific geometric shapes (disc, ellipse or polygon), the intersections between fractures, and a relatively high flow velocity will produce more head losses when fluids flow through fractures and these losses cannot be studied by the rectangular parallel plate experiments.

$$\frac{\Delta H_{s\_exp}}{\Delta H_{in-out\_exp}}\% = 1.275\frac{b^{0.614}Q^{0.309}}{L^{0.589}} R^2 = 0.958 \quad (5)$$

2.2 Local head losses occurred on the fracture intersections

To explore the composition of ΔH_{s_exp}, the numerical simulation approach and an estimation method are applied together in the following study. In order to avoid the strong disturbance in the constriction area near the edge of the disc, the piezometer was placed a certain distance (4 cm in this experiment) away from the intersection. As a result, under this circumstance, the validity and credibility of the numerical modelling were first verified by comparing the observed experimental and simulated numerical results of the head losses between two piezometers for a few investigation scenarios with lower average flow velocity. As mentioned, totally 40 numerical models based on the same hydraulic conditions as the experimental scenarios were established. Through numerical simulations,

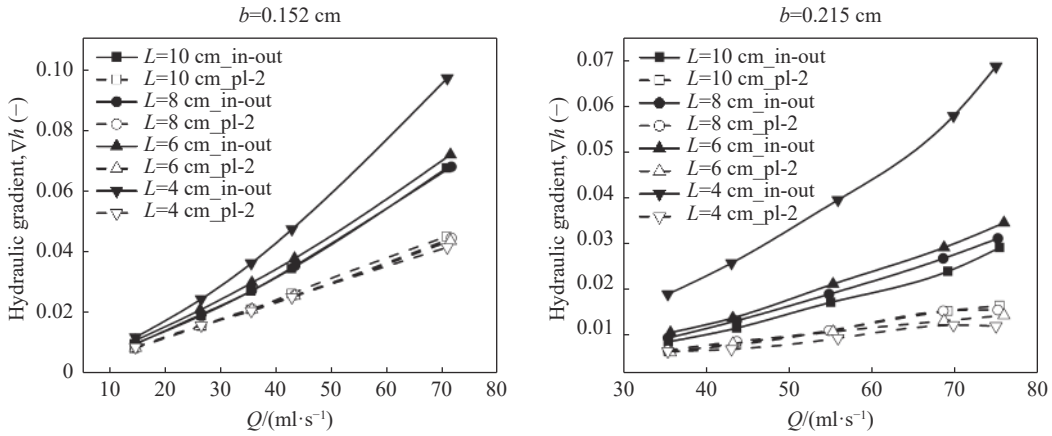

Fig. 4 The relationships between the hydraulic gradient (∇H_{in-out_exp} and ∇H_{p1-2_exp}) and the flow rate (Q) in different experimental scenarios

Table 2 The experimental results of ΔH_{in-out_exp} and ΔH_{p1-2_exp} along with the percentage of ΔH_{s_exp} to ΔH_{in-out_exp}

	***b*=0.152 cm**				***b*=0.215 cm**			
	Q **(cm³/s)**	ΔH_{in-out_exp} **(cm)**	ΔH_{p1-2_exp} **(cm)**	$\frac{\Delta H_{s\_exp}}{\Delta H_{in-out\_exp}}$ **(-)**	***Q*** **(cm³/s)**	ΔH_{in-out_exp} **(cm)**	ΔH_{p1-2_exp} **(cm)**	$\frac{\Delta H_{s\_exp}}{\Delta H_{in-out\_exp}}$ **(-)**
L=10 cm	14.41	0.48	0.34	29.17%	35.34	0.45	0.29	35.56%
	26.53	0.95	0.65	31.58%	43.55	0.60	0.35	41.67%
	35.54	1.35	0.88	34.81%	54.91	0.88	0.48	45.45%
	42.88	1.72	1.10	36.05%	69.03	1.22	0.66	45.90%
	70.97	3.38	1.89	44.08%	75.28	1.48	0.71	52.03%
L=8 cm	14.53	0.47	0.35	25.53%	35.28	0.49	0.30	38.78%
	26.54	0.97	0.66	31.96%	43.57	0.68	0.38	44.12%
	35.68	1.36	0.89	34.56%	54.70	0.97	0.48	50.52%
	43.51	1.77	1.08	38.98%	68.48	1.36	0.66	51.47%
	71.83	3.40	1.87	45.00%	75.06	1.58	0.67	57.59%
L=6 cm	14.61	0.54	0.35	35.19%	35.58	0.55	0.28	49.09%
	26.30	1.04	0.65	37.50%	43.10	0.71	0.36	49.30%
	35.68	1.49	0.88	40.94%	55.17	1.08	0.47	56.48%
	43.43	1.89	1.07	43.39%	68.55	1.48	0.57	61.49%
	71.66	3.60	1.83	49.17%	75.78	1.75	0.62	64.57%
L=4 cm	14.61	0.59	0.36	38.98%	35.25	0.97	0.29	70.10%
	26.51	1.22	0.66	45.90%	42.94	1.31	0.31	76.34%
	35.57	1.81	0.86	52.49%	55.76	2.00	0.41	79.50%
	42.94	2.37	1.05	55.70%	69.71	2.92	0.53	81.85%
	71.07	4.86	1.74	64.20%	74.82	3.46	0.52	84.97%

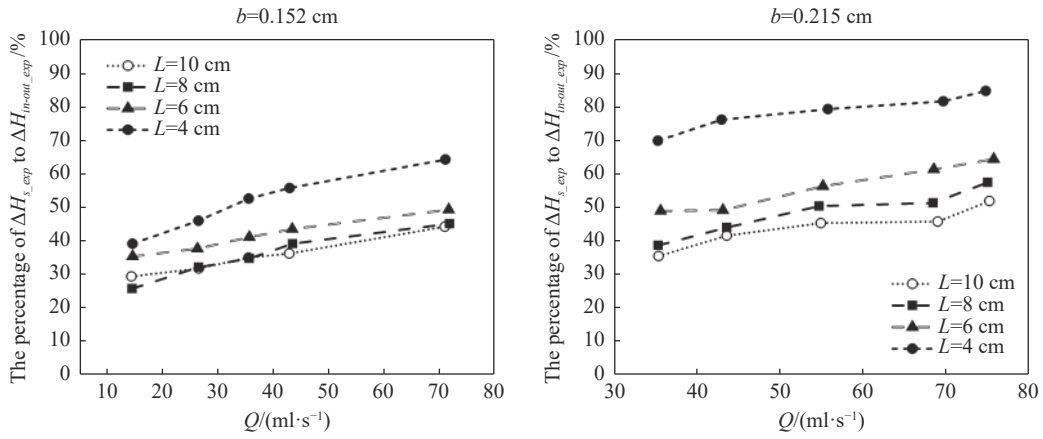

Fig. 5 The percentage of ΔH_{s_exp} to ΔH_{in-out_exp} in different experimental scenarios

the linear head loss within a fracture in each experimental scenario was identified. Finally, the additional local head loss (ΔH_{i_der}) caused on the intersections between the fractures was estimated by integrating the experimental results using following Equations (6) and (7).

$$\Delta H_{in-out\_der} = \frac{\Delta H_{in-out\_num}}{\Delta H_{p1-2\_num}} \times \Delta H_{p1-2\_exp} \quad (6)$$

$$\Delta H_{i\_der} = \Delta H_{in-out\_exp} - \Delta H_{in-out\_der} \quad (7)$$

Where: ΔH_{in-out_num} represents the linear head loss between the inlet and the outlet obtained by numerical simulation; ΔH_{p1-2_num} represents the linear head loss between two piezometers, achieved also though numerical simulations. Additionally, ΔH_{in-out_der} represents the extrapolated total head loss from ΔH_{p1-2_exp} by estimation according to the proportional relationship between ΔH_{p1-2_num} and ΔH_{in-out_num}. It primarily consists of the linear head loss (ΔH_l) and the additional head loss on

fracture plane (ΔH_n) which has already considered the effects caused by the dominant flow area. However, this value may be underestimated, because the ΔH_n close to the intersections should be larger than the extrapolated one based on the linear estimation due to a relatively high velocity in this shrink area. Therefore, the derived value of ΔH_{i_der} would be a conservative estimation or an upper bound of the additional local head loss caused on the intersections between the fractures.

According to the above procedure and method, the derivate results of ΔH_{in-out_der} and $\frac{\Delta H_{i\_der}}{\Delta H_{in-out\_exp}}$ for the 40 experiments were calculated and listed in the following table (Table 3).

By comparing Table 2 with Table 3, it can be seen that the values of ΔH_{p1-2_num} and $\Delta H_{p1-2\_\_exp}$ are very similar, while minor difference could be observed. The numerical simulation results are often smaller than the observed experimental ones, particularly for the cases with larger intersection lengths, and the difference between ΔH_{p1-2_exp} and ΔH_{p1-2_num} would become larger with the increase of the flow rate. That is because the dominant flow area becomes lager and most of the fracture plane is involved in fluid flow when intersection is large (Fig. 6). In this situation ΔH_n would be the main additional head loss and it increases with the increase in fluid velocity.

From Fig. 7, it can be seen that the percentage of $\frac{\Delta H_{i\_der}}{\Delta H_{in-out\_exp}}$ increases with both apertures and flow rates, while decreases with intersection lengths. In this study, the percentage value ranges from 0 to 73.57%, which indicates that the local head loss caused by the intersection varies greatly in different situations so that it is necessary to consider the impacts of fracture intersection in field investigations. For example, when performing pumping tests in fractured rocks, the ΔH_i on the intersection between the fractures should be given special attention as this additional loss might be very large.

Likewise, the following non-linear regression equation of power function is the best fit comparing with several other possible function types such as linear, exponential, logarithmic, polynomial, and power functions. Equation (8) quantitatively describes the statistical relationship between that percentage and those controlling variables. The goodness of fit corresponding to the regression equation is as high as 0.934.

Table 3 The derivate results of ΔH_{in-out_der} and the ratios of ΔH_{i_der} to ΔH_{in-out_exp}

	***b*=0.152 cm**				***b*=0.215 cm**			
	Q **(cm^3/s)**	$\frac{\Delta H_{in-out\_num}}{\Delta H_{p1-2\_num}}$ **(-)**	ΔH_{in-out_der} **(cm)**	$\frac{\Delta H_{i\_der}}{\Delta H_{in-out\_exp}}$ **(-)**	***Q*** **(cm^3/s)**	$\frac{\Delta H_{in-out\_num}}{\Delta H_{p1-2\_num}}$ **(-)**	ΔH_{in-out_der} **(cm)**	$\frac{\Delta H_{i\_der}}{\Delta H_{in-out\_exp}}$ **(-)**
L=10 cm	14.41	1.46	0.49	0.00%	35.34	1.46	0.42	6.23%
	26.53	1.46	0.95	0.44%	43.55	1.46	0.52	15.12%
	35.54	1.46	1.28	5.15%	54.91	1.46	0.69	20.63%
	42.88	1.46	1.60	6.94%	69.03	1.46	0.97	21.28%
	70.97	1.46	2.74	18.65%	75.28	1.46	1.04	30.20%
L=8 cm	14.53	1.52	0.54	0.00%	35.28	1.52	0.47	6.96%
	26.54	1.52	1.00	0.00%	43.57	1.52	0.58	15.08%
	35.68	1.52	1.36	0.55%	54.70	1.52	0.72	24.81%
	43.51	1.52	1.65	7.27%	68.48	1.52	1.01	26.25%
	71.83	1.52	2.84	16.42%	75.06	1.52	1.03	35.56%
L=6 cm	14.61	1.61	0.57	0.00%	35.58	1.61	0.46	17.90%
	26.30	1.61	1.05	0.00%	43.10	1.61	0.57	18.23%
	35.68	1.61	1.41	4.76%	55.17	1.61	0.76	29.82%
	43.43	1.61	1.73	8.70%	68.55	1.61	0.92	37.90%
	71.66	1.61	2.96	18.02%	75.78	1.61	1.01	42.87%
L=4 cm	14.61	1.76	0.63	0.00%	35.25	1.76	0.52	47.42%
	26.51	1.76	1.16	4.85%	42.94	1.76	0.54	58.38%
	35.57	1.76	1.51	16.44%	55.76	1.76	0.73	63.95%
	42.94	1.76	1.85	22.09%	69.71	1.76	0.94	68.08%
	71.07	1.76	3.06	37.05%	74.82	1.76	0.91	73.57%

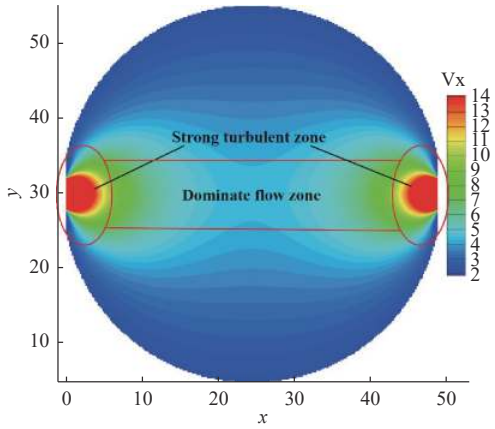

Fig. 6 The strong turbulent area and dominant flow area in a disc-shaped fracture

$$\frac{\Delta H_{i\_der}}{\Delta H_{in-out\_exp}}\% = 3.457\frac{b^{2.456}Q^{0.981}}{L^{1.395}} R^2 = 0.934 \quad (8)$$

2.3 Implications

Studying the statistical relationships between the additional losses (ΔH_n and ΔH_i) and their controlling variables could provide a simplified method for correcting the traditional numerical models based on linear flow governing equations. The two regression equations presented above were obtained under the specific conditions of the experiments in this study, while the expressions including the exponents of the variables should vary if the experimental features change such as the diameter of the disc-shaped fracture and locations of intersection lines for the flow inlet and outlet in a fracture. However, the regression model type and the changing trend of these two percentages with their controlling variables are expected to be similar to those obtained in this investigation. Indeed, the research process and method applied in this study can be summarized as a general approach which could be implemented in the same kind of head loss investigations when addressing different features of the disc-shaped fracture such as the diameter of the disc-shaped fracture and locations of intersection lines for the flow inlet and outlet.

In the general approach, specifically, the first step is to set up a physical fracture flow model. The second step is to obtain the total head loss on the intersections and their vicinity through the laboratory experiments. Third, the corresponding numerical models should then be established. Fourth, by integrating the numerical simulation results, a conservative estimation or upper bound of the additional local head loss occurred on the intersections can be determined. Finally, the appropriate regression models can be further established between these losses and their controlling factors to quantitively describe their statistical relationships.

3 Conclusions

In this paper, a disc-shaped fracture model was adopted to investigate total head losses occurred on and nearby the intersections and local head losses occurred on the intersections using experimental and numerical methods. Compared with the rectangular parallel plates model, the velocity distribution in this disc-shaped fracture is more complicated. The following primary conclusions could be drawn based on this investigation.

(1) The total head loss (ΔH_{s_exp}) produced on and nearby the intersections between the disc-shaped fractures accounts for 29.17% - 84.97% of the entire total head loss (ΔH_{in-out_exp}) in a fracture, indicating that a rather large proportion of the total head loss could occur over a small part of the whole flow area in a disc-shaped fracture. Moreover, this proportion or percentage $\left(\frac{\Delta H_{s\_exp}}{\Delta H_{in-out\_exp}}\%\right)$ consistently presents an increasing trend with the

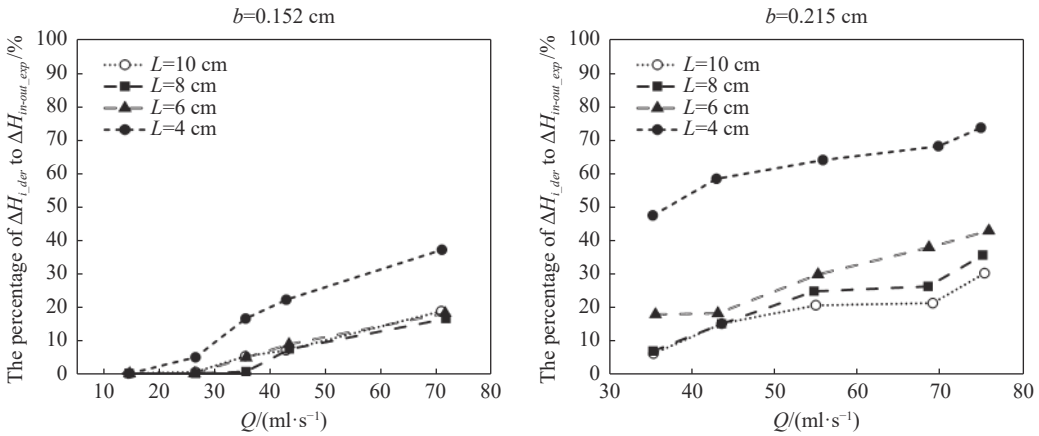

Fig. 7 The percentage of ΔH_{i_der} to ΔH_{in-out_exp} in different experimental scenarios

increase of b and Q, and the decrease of L. Specifically, this proportion can be statistically described by a power function with the variables b, L, and Q , from which a high coefficient of determination was achieved

(2) The additional local head loss represented by ΔH_i, occurred on the intersections between fractures, was investigated by implementing both the laboratory experiments and numerical simulations. The results showed that the ΔH_{i_der} increases when the aperture and the flow rate increase and decreases with the intersection length. In addition, the percentage of ΔH_{i_der} to ΔH_{in-out_exp} ranges from 0 to 73.57%. Moreover, this percentage could be statistically explained by a power function with the pertaining variables b, L, and Q and a high coefficient of determination was achieved. This investigation reveals that the additional head losses on intersections between fractures vary greatly in different flow situations, so that they should be necessarily considered for groundwater modeling in fractured rocks.

(3) This study puts forward a general approach for investigating head losses on and nearby the intersections between disc-shaped fractures, which can be implemented in other similar researches with different conditions such as different fracture geometrical parameters. This kind of investigation may provide a "bridge" to adjust or correct head losses computed from application of linear flow model while non-linear flow exists in a disc-shipped fracture.

Acknowledgements

This study was supported by National Key Research and Development Program of China (No. 2020 YFC1807100, No. 2019YFC1806205) and National Natural Science Foundation of China (No. 41572 240).

Appendix A

The components and classification of each head loss mentioned in this paper

	Major loss		Minor loss
	ΔH_l	ΔH_n	ΔH_i
ΔH_{in-out_exp}	√	√	√
ΔH_{p1-2_exp}	√	√	
ΔH_{s_exp}	√	√	√
ΔH_{in-out_der}	√	√	
ΔH_{i_der}			√
ΔH_{in-out_num}	√		
ΔH_{p1-2_num}	√		

The explanation list of each head loss in this paper:

ΔH_l: the head loss in linear laminar flow along the flow path.

ΔH_n: the head loss in non-linear flow along the flow path, which represents the non-linear part. The sum of ΔH_l and ΔH_n is the traditional frictional head loss.

ΔH_i: the local head loss on the intersections of the fractures.

ΔH_{p1-2_exp}: the total head loss between two piezometers in the experiments.

ΔH_{in-out_exp}: the total head loss between two intersections (inlet and outlet) in the experiments.

ΔH_{s_exp}: the total head loss on and nearby the intersections in the experiments which is equal to the difference between ΔH_{in-out_exp} and ΔH_{p1-2_exp}.

ΔH_{in-out_num}: the linear laminar head loss within two intersections (inlet and outlet) which obtained from numerical simulations.

ΔH_{p1-2_num}: the linear laminar head loss within two piezometers which obtained from numerical simulations.

ΔH_{in-out_der}: the derived total frictional head loss within two intersections which contains two parts of ΔH_l and ΔH_n.

ΔH_{i_der}: the derived local head loss exactly on the intersections.

References

Baecher GB, Lanney NA. 1978. Trace length biases in joint surveys, 19th U. S. Symposium on Rock Mechanics: 56–65.

Bear. 1972. Dynamics of fluids in porous media, Dover Publications.

Borgne TL, Bour O, Paillet FL, et al. 2006. Assessment of preferential flow path connectivity and hydraulic properties at single-borehole and cross-borehole scales in a fractured aquifer. Journal of Hydrology, 328(1-2): 347-359.

Cacas MC. 1990. Modeling fracture flow with a stochastic discrete fracture network: Calibration and Validation 1. The flow model. Water Resources Research, 26(3): 491-500.

Cao C, Xu ZG, Chai JR, et al. 2019. Radial fluid flow regime in a single fracture under high hydraulic pressure during shear process. Journal of Hydrology, 579: 124-142.

Dershowitz WS, Einstein HH. 1988. Characterizing rock joint geometry with joint system

models. International Journal of Rock Mechanics and Mining Sciences & Geomechanics Abstracts, 21(1): 21-51.

Dverstorp B, Andersson J, Nordqvist W. 1992. Discrete fracture network interpretation of field tracer migration in sparsely fractured rock. Water Resources Research, 28(9): 2327-2343.

Gong Y, Mehana M, El-Monier I, et al. 2020. Proppant placement in complex fracture geometries: A computational fluid dynamics study. Journal of Natural Gas Science and Engineering, 79: 103295.

Grechka V, Kachanov M. 2006. Effective elasticity of rocks with closely spaced and intersecting cracks. Geophysics. 71: 85-91. https://doi.org/10.1190/1.2197489

Guo JC, Zheng J, Lyu Q, et al. 2020. A procedure to estimate the accuracy of circular and elliptical discs for representing the natural discontinuity facet in the discrete fracture network models. Computers and Geotechnics, 121: 103483.

Hartley L, Roberts D. 2013. Summary of discrete fracture network modelling as applied to hydrogeology of the Forsmark and Laxemar sites, Swedish: 8-9.

Hunter Rouse. 1946. Elementary mechanics of fluids. New York, John Wiley & Sons, Inc. Chapter, 7: 192-226.

Hu YJ, Mao GH, Cheng WP, Zhang JJ. 2005. Theoretical and experimental study on flow distribution at fracture intersections,. Journal of Hydraulic Research, 43(3): 321-327.

Jing LR. 2007. The basics of fracture system characterization – Field mapping and stochastic simulations. Developments in geotechnical engineering, 85: 147-177.

Johnson J, Brown S, Stockman H. 2006. Fluid flow and mixing in rough-walled fracture intersections. Journal of Geophysical Research: Solid Earth, 111(B12). https://doi.org/10.1029/2005jb004087

Kemler E. 1933. A study of the sata on the flow of fluid in pipes. Transactions of the ASME. 55 (Hyd-55-2): 7–32.

Kolditz O. 2001. Non - linear flow in fractured rock. International Journal of Numerical Methods for Heat & Fluid Flow, 11(6): 547-575.

Koudina N, Gonzalez Garcia R, Thovert JF, et al. 1998. Permeability of three-dimensional fracture networks. Physical Review E, 57(4): 4466-4479.

Lei Q, Latham JP, Tsang CF. 2017. The use of discrete fracture networks for modelling coupled geomechanical and hydrological behaviour of fractured rocks. Computers and Geotechnics, 85: 151-176.

Liu R, Jiang Y, Li B. 2016. Effects of intersection and dead-end of fractures on nonlinear flow and particle transport in rock fracture networks. Geosciences Journal, 20(3): 415-426.

Long JCS, Gilmour P, Witherspoon PA. 1985. A model for steady fluid flow in random three-dimensional networks of disc-shaped fractures. Water Resources Research, 21(8): 1105-1115.

Moody LF, Princeton NJ. 1944. Friction factors for pipe flow. Transactions of the ASME, 66: 671-684.

Petchsingto T, Karpyn ZT. 2009. Deterministic modeling of fluid flow through a CT-scanned fracture using computational fluid dynamics. Energy Sources, Part A: Recovery, Utilization, and Environmental Effects, 31(11): 897–905. https://doi.org/10.1080/15567030701752842

Pollard DD. 1976. On the form and stability of open hydraulic fractures in the earth's crust. Geophysical Research Letters, 3(9): 513-516.

Pruess K. 1998. On water seepage and fast preferential flow in heterogeneous, unsaturated rock fractures. Journal of Contaminant Hydrology, 30(3-4): 333-362.

Reza J, Maria K et al. 2018. A multi-scale approach to identify and characterize preferential flow paths in a fractured crystalline rock. Proceedings of the 52nd U. S. Rock Mechanics/Geomechanics Symposium 17-20, Seattle: Washington.

Su GW, Geller JT, Pruess K et al. 2001. Solute transport along preferential flow paths in unsaturated fractures. Water Resources Research, 37(10): 2481-2491.

Tuckwell GW, Lonergan L, Jolly RJH. 2003. The control of stress history and flaw distribution on the evolution of polygonal fracture net-

works. Journal of Structural Geology 25(8): 1241–1250. https://doi.org/10.1016/S0191-8141(02)00165-7

Vu MN, Pouya A, Seyedi DM. 2018. Effective permeability of three-dimensional porous media containing anisotropic distributions of oriented elliptical disc-shaped fractures with uniform aperture. Advances in Water Resources, 118: 1-11.

Wang M, Kulatilake PHSW, Um J, et al. 2002. Estimation of REV size and three dimensional hydraulic conductivity tensor for a fractured rock mass through a single well packer test and discrete fracture fluid flow modeling. International Journal of Rock Mechanics and Mining Sciences, 39(7): 887-904.

Wang Y, Liu YG, Bian K, et al. 2020. Seepage-heat transfer coupling process of low temperature return water injected into geothermal reservoir in carbonate rocks in Xian County, China. Journal of Groundwater Science and Engineering, 8(4): 305-314.

Wilson CR, Witherspoon PA. 1976. Flow interference effects at fracture intersections. Water Resources Research, 12(1): 102-104.

Witherspoon PA, Wang JSY, Gale JE. 1980. Validity of cubic law for fluid flow in a deformable rock fracture. Water Resources Research, 16(6): 1016-1024.

Xiong F, Wei W, Xu C, et al. 2020. Experimental and numerical investigation on nonlinear flow behaviour through three dimensional fracture intersections and fracture networks. Computers and Geotechnics, 121, May 103446. https://doi.org/10.1016/j.compgeo.2020.103446

Zimmerman RW, Al-Yaarubi A, Pain CC, et al. 2004. Non-linear regimes of fuid fow in rock fractures. International Journal of Rock Mechanics and Mining Sciences, 41(1): 1-7.

Zhang Z, Nemcik J, Ma S. 2013. Micro- and macro-behaviour of fluid flow through rock fractures: An experimental study. Hydrogeology Journal, 21(8): 1717-1729.